Journal of Applied Science, Engineering, Technology, and Education *ISSN: 2685-0591 (online)*
Vol. 8 No. 2 (2026)
https://doi.org/10.35877/454RI.asci4869

Optimization of Reaction Turbine via Central Composite Design: A Parametric Analysis

Alberto E. Lastimado Jr. [a,b,c*], Enrique D. Festijo [a,d], Abigail P. Cid-Andres[a], Ginno L. Andres[a]

[a]*Doctor in Engineering Management Program, Polytechnic University of the Philippines- Open University System, Anonas St., Sta. Mesa, Manila, 1016, Philippines*
[b]*Engineering Department, North Eastern Mindanao State University – Bislig Campus, Maharlika, Bislig City, 8311, Philippines*
[c]*Knowledge and Technology Transfer Office, North Eastern Mindanao State University – Tandag Campus, Tandag City, 8300, Philippines*
[d]*Technological Institute of the Philippines, Manila, Philippines*

Abstract

The study comprehensively investigates hydrodynamic performance, parameter optimization, and scaling implications of a 10-inch-high Cone-Enhanced Split Reaction Turbine (CESRT). To systematically decode the multi-variable design space without incurring prohibitive experimental costs, the study employs a highly structured Central Composite Design (CCD) matrix nested deeply within the Response Surface Methodology (RSM) framework, the analysis evaluates the independent, quadratic, and interactive effects of three critical operational parameters: applied torque, system bypass angle, and internal cone size. The statistical model demonstrated exceptional predictive reliability, characterized by an F-value of 319.59 and a coefficient of determination (R^2) of 0.9976. The empirical findings reveal that while applied torque serves as the primary driver of operational efficiency, complex, non-linear interactions exist between the torque, the bypass angle governing the inlet flow, and the geometric influence of the internal cone modifier. Maximum hydraulic efficiency for the 10-inch architecture is achieved at an applied torque of 60 N-m, a bypass angle of 22.5°, and a cone size of 2.5 inches, yielding a peak predicted efficiency of 64.5803%. Crucially, a comparative scaling analysis against preceding 8-inch CESRT configurations reveals a significant degradation in isentropic efficiency associated with the increased aspect ratio of the 10-inch model. These findings demonstrate mathematically that radial expansion, rather than vertical elongation, is hydrodynamically optimal for simple reaction turbomachinery.

Keywords: Central Composite Design; Energy conversion; Numerical Optimization; Pico-hydropower; Split reaction turbine.

Received: 7 June 2026 Revised: 12 July 2026 Published: 31 August 2026

1. Introduction

The contemporary global energy landscape is characterized by a critical and persistent dichotomy: the urgent, climate-driven mandate to transition toward renewable energy architectures, juxtaposed against the enduring challenge of energy poverty in geographically isolated and developing regions (Ibekwe et al., 2024). As centralized power grids remain economically and logistically unfeasible for thousands of off-grid communities, decentralized energy generation has emerged as a fundamental pillar of sustainable economic development and environmental stewardship. Within this decentralized matrix, pico-hydropower—defined strictly as hydroelectric generation systems producing less than 5 kW of electrical output, represents one of the most reliable, cost-effective, and environmentally benign solutions currently available (Journals et al., 2015). Unlike solar photovoltaic or wind energy systems, which suffer from pronounced diurnal and seasonal intermittency requiring massive battery storage systems, pico-hydropower systems can provide continuous, reliable baseload electricity, provided a consistent run-of-river or low-head water source is available (Williamson et al., 2019). Furthermore, the localized, small-scale nature of these installations results in a negligible ecological footprint, entirely bypassing the severe environmental degradation, aquatic habitat disruption, social displacement, and massive capital expenditures associated with conventional, large-scale, dam-based hydroelectric infrastructure (Lange et al., 2019).

* Corresponding author.
E-mail address: alastimado@nemsu.edu.ph

Despite the profound theoretical advantages of pico-hydropower, the widespread, global deployment of these systems is frequently obstructed by a combination of high initial specific costs, the strict necessity for highly site-specific engineering, and the inherently variable nature of low-head water resources. To ensure the long-term economic viability and technical robustness of pico-hydro installations, particularly in rural communities lacking advanced technical expertise or sophisticated manufacturing bases, the utilized turbine designs must prioritize extreme structural simplicity. They must be capable of utilizing locally sourced or readily available commercial materials without sacrificing the mechanical efficiency required to extract meaningful power from low-energy fluid streams (Lastimado et al., 2025; Williamson et al., 2019).

In response to these rigid operational constraints, the Split Reaction Turbine (SRT) has emerged as a highly promising technology optimized specifically for low-head and ultra-low-head hydro resources (typically operating at hydraulic heads between 0.5 and 3.0 meters). The SRT operates on a fundamentally elegant application of Newton's third law of motion and the conservation of angular momentum. Incoming pressurized water flows axially into the vertical base of the turbine housing, where it is bifurcated into two separate fluid streams (Chica & Rubio-Clemente, 2017; Sobel et al., 2025). These streams are subsequently discharged tangentially through opposing, offset vertical exit nozzles. The dramatic change in fluid momentum as the water accelerates through the restrictive nozzles generates a reactive thrust vector, which induces high-speed rotation in the entire turbine assembly. This inherently simple design eradicates the need for the complex, precision-machined stator guide vanes, scroll casings, or complex blade profiles found in traditional Francis, Turgo, or Kaplan turbines (Barsi et al., 2019). Consequently, the SRT can be manufactured utilizing standard polyvinyl chloride (PVC) pipe fittings and basic, low-skill fabrication techniques, drastically lowering the barrier to entry (Lastimado et al., 2025).

While early foundational studies established the baseline viability of the SRT—achieving overall efficiencies in the range of 65% to 70% under controlled, ultra-low-head conditions (Subekti et al., 2022)—these iterations often suffered from severe internal hydraulic losses, primarily resulting from abrupt flow separation, internal boundary layer turbulence, and suboptimal momentum transfer within the unguided core of the cylindrical housing. To systematically mitigate these internal inefficiencies, recent engineering efforts have focused heavily on the integration of internal flow modifiers (Zhussupbekov et al., 2025). The advent of the Cone-Enhanced Split Reaction Turbine (CESRT) represents a significant hydrodynamic leap forward. By positioning a geometrically optimized, conical insert directly within the vertical flow path, the CESRT strategically accelerates and smoothly directs the fluid outward toward the exit nozzles, significantly reducing the volume of stagnant water (dead zones) and minimizing turbulent kinetic energy dissipation (Lastimado et al., 2025).

A critical gap in the existing scientific literature, however, pertains to the volumetric and geometric scaling laws governing these simple reaction turbines. While extensive research has successfully optimized specific cone geometries for baseline turbine heights (e.g., standard 8-inch vertical housing), the complex hydrodynamic impact of altering the turbine's overall height-to-diameter ratio—often referred to as the aspect ratio—remains largely unexplored in the specific context of the CESRT architecture (Hunt et al., 2024; Lastimado et al., 2025). While classical turbomachinery design relies heavily on established affinity laws and geometric similitude—where performance scales predictably with impeller diameter and rotational speed—the application of these universal principles to unconventional, ultra-low-head pico-hydro architectures remains sparsely documented. Traditional scaling heuristics for large-scale reaction turbines strictly prioritize radial expansion to maximize the moment arm for torque generation. However, the drive for low-cost, decentralized manufacturing in developing regions often tempts field engineers to scale systems volumetrically by simply altering aspect ratios (e.g., utilizing longer standard commercial pipe lengths). This creates a critical need to bridge the gap between theoretical turbomachinery physics and low-cost prototyping, empirically validating whether classical radial scaling heuristics must universally govern these simplified, decentralized topologies on a global scale. Classical turbomachinery theory strictly dictates that altering the aspect ratio of a fluid passage fundamentally alters the operational Reynolds number, the boundary layer thickness along the wetted perimeter, and the manifestation of energy-robbing secondary flow vortices, all of which heavily dictate the machine's ultimate isentropic efficiency (Sebastián et al., 2021; Sobel et al., 2025). Addressing this specific, critical knowledge gap, the present study undertakes a rigorous optimization analysis of a modified CESRT, deliberately scaled and fabricated to a 10-inch height.

The primary objective of this research is to systematically decode the highly coupled interplay between the applied mechanical load (torque), the bypass valve angle (which regulates absolute flow dynamics and pressure head), and the internal cone size within this elongated, higher-aspect-ratio geometry. To achieve a comprehensive, mathematically sound understanding of this multi-variable design space without incurring the prohibitive financial costs of full-factorial empirical testing, this research employs a Central Composite Design (CCD) matrix nested deeply within the Response Surface Methodology (RSM) framework.

2. Materials and Methods

2.1. Turbine Design and Specifications

The physical prototype utilized for this rigorous empirical investigation is a specifically modified 10.0-inch Cone-Enhanced Split Reaction Turbine (CESRT) adapted from the study of Lastimado et al. (2025). The foundational structural design rigidly adheres to the overarching principles of simplicity, low capital cost, and manufacturability. The primary cylindrical envelope is constructed from a standard, commercially available PVC pipe shown in Figure 1. The selection of PVC is highly deliberate; it is inherently resistant to aquatic corrosion, exceptionally lightweight, and fundamentally symmetrical. This perfect radial symmetry virtually eliminates the need for complex, expensive dynamic balancing procedures required in traditional cast-metal impellers (Mansour et al., 2024).

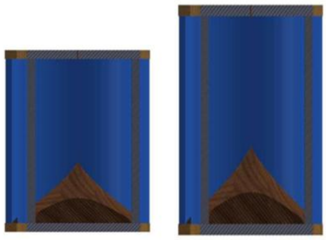

Fig. 1. Turbine design (Adopted from the study of Lastimado et. al. (2025))

The fabrication protocol involves vertically splitting the PVC cylinder into two perfectly equal semicircular halves (Lastimado et al., 2025). These halves are then precisely reattached to solid, structurally rigid top and bottom cover plates with a deliberate geometric offset. This offset creates two diametrically opposed, continuous vertical slots running the entire 10-inch height of the turbine; these slots function as the high-velocity fluid exit nozzles (Lastimado et al., 2025). The exact dimensional specifications defining the cylindrical envelope of the tested 10-inch CESRT are total internal height (h) 10.0 inches, outer diameter (d) 7.5 inches, and cover plate thickness (t) 0.50 inches (for both the top and base boards).

To actively manipulate internal fluid dynamics, removable central cones precision-lathed from locally sourced mahogany wood are integrated. The base radius of all tested cones is rigidly fixed at $r = 3.75$ inches. This precise dimension matches the internal radius of the PVC housing, ensuring a watertight seal at the base plate to prevent parasitic leakage beneath the cone (Lastimado et al., 2025). The experimental design dictates testing specific cone heights ranging from a minimum extreme of 2.25 inches to a maximum extreme of 3.25 inches.

2.2. Experimental Setup and Procedure

To systematically evaluate the hydraulic efficiency of the 10-inch CESRT under steady-state thermodynamic conditions, a closed-loop, recirculating hydrodynamic test rig was employed as shown in Figure 2. This system utilizes a substantial primary water reservoir that acts as the physical housing for the turbine and provides immense fluid thermal mass to maintain steady fluid density. High-capacity engine pumps deliver a consistent, high-pressure mass flow of water directly into the base of the turbine housing via a specifically engineered orifice equipped with a high-tolerance rotary seal.

To simulate the inherent variability of real-world run-of-river flow rates, a precision ball valve is integrated into a bypass line. By precisely adjusting the bypass angle, the mass flow rate and absolute pressure delivered to the turbine inlet can be seamlessly modulated without altering primary pump speeds. The mechanical power output extracted by the CESRT is precisely quantified using a calibrated electrodynamometer coupled to the upper drive shaft via a rigid flange connection. The electrodynamometer applies specific resistive mechanical loads while a digital tachometer records resultant rotational velocity (RPM).

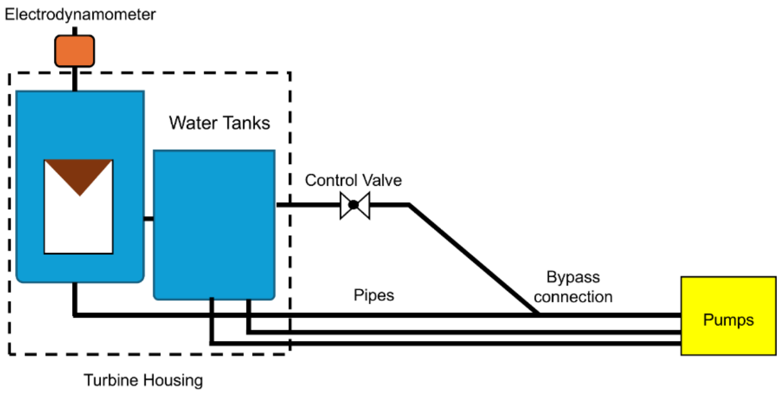

Fig. 2. Experimental Setup of CESRT

The theoretical framework for calculating the system's total hydraulic efficiency (n) relies on determining the ratio of the mechanical power output to the hydraulic power input, defined by the following fundamental fluid dynamic eq. 1, eq. 2, and eq. 3:

$$P_{input} = \rho \cdot g \cdot Q \cdot H \tag{1}$$

$$P_{output} = \frac{2\,\pi\,TN}{60} \tag{2}$$

$$n_t = \frac{P_{output}}{P_{input}} x\ 100\% \tag{3}$$

where ρ represents the density (kg/m^3), g the gravitational acceleration due to gravity (m/s^2), Q the volume flow rate (m^3/s), H is the head, T is the torque (N-m), N is the speed (rpm), and n_t the turbine efficiency.

2.3. Design of Experiment and Statistical Analysis

To isolate optimal operational parameters efficiently, the study utilized a three-factor Central Composite Design (CCD) under the Response Surface Methodology (RSM) umbrella (Lastimado et al., 2025; Palanikumar, 2021; Yeswanth, 2025). This specific design framework was chosen because it drastically reduces the required experimental runs compared to traditional exhaustive methods. Specifically, evaluating three continuous factors across five distinct levels (-α, -1, 0, +1, +α) using a full factorial design would strictly necessitate 125 discrete experimental runs (5^3). By employing the CCD matrix, the total requirement was systematically reduced to just 17 carefully positioned runs (comprising 8 factorial points, 6 axial/star points, and replicated center points). This results in a savings of 108 experimental runs—an 86.4% reduction in resource and time expenditure—while still retaining complete mathematical orthogonality and the statistical rigor necessary to confidently fit a full second order (quadratic) predictive model (Njoku & Otisi, 2023). The three independent continuous variables utilized are depicted in Table 1.

Table 1. Coded factors for CCD

Factor	**Level**					
	Coded symbol	-α	-1	0	+1	+α
Torque (N · m)	A	0	20	40	60	80
Bypass-angle (θ)	B	0	22.5	45	67.5	90
Cone size (in.)	C	2.25	2.5	2.75	3.0	3.25

The complex relationship between these variables (X_1, X_2, X_3) and the target response variable (Efficiency, Y) is approximated utilizing a second-order polynomial regression of eq. 4 (Kayarogannam et al., 2022; Lastimado et al., 2025; Sobel et al., 2025):

$$Y = \beta_0 + \sum_{i=1}^{k} \beta_i X_i + \sum_{i=1}^{k} \beta_{ii} X_i^2 + \sum_{i=1}^{k-1} \sum_{j=i+1}^{k} \beta_{ij} X_i X_j + \epsilon \quad (4)$$

where β_0 represents the intercept constant, β_i represents the linear coefficients for each factor, β_{ii} denotes the quadratic coefficients representing the parabolic curvature of the response, β_{ij} signifies the interaction coefficients between varying factors, and ϵ represents the residual statistical error.

3. Results and Discussion

3.1. Experimental Performance and ANOVA

A total of 17 discrete experimental runs were successfully executed following the CCD sequence. Empirical data immediately highlighted extreme variance in system efficiency across the defined operational envelope. The absolute minimum efficiency recorded was a mere 14.265% during a zero-torque freewheeling state where massive kinetic energy losses occur. Conversely, the maximum empirical efficiency achieved was 65.015% at a maximum axial load of 80 N-m. Furthermore, the negligible variance across replicated centre points (clustered tightly between 46.381% and 47.210%) proved the immense stability of the closed-loop thermodynamic test rig.

The overall Model F-value was calculated at a massive 319.59, firmly and unequivocally establishing the statistical significance of the regression shown in Table 2. In practical statistical terms, there is merely a 0.01% probability that this variance magnitude could manifest purely through stochastic system noise. ANOVA revealed that all primary linear terms—Torque (A), Bypass-angle (B), and Cone Size (C)—are highly significant contributors to efficiency variance. Torque exhibited an overwhelming F-value of 2500.55, indicating it is by far the most dominant main effect. Pure quadratic terms (A^2, B^2, and C^2) all yielded p-values well below the 0.05 threshold, definitively proving a non-linear relationship and mathematically justifying the second-order CCD polynomial. Additionally, the non-significant Lack of Fit test outcome ($p = 0.1196$) confirmed that the chosen quadratic model adequately captures the response surface without overfitting data noise.

Table 2. ANOVA for the Quadratic Response Surface Model targeting Efficiency

Source	Sum of Squares	df	Mean Square	F-value	p-value	
Model	3049.26	9	338.81	319.59	< 0.0001	significant
A-Torque	2650.93	1	2650.93	2500.55	< 0.0001	
B-Bypass-angle	95.68	1	95.68	90.25	< 0.0001	
C-Cone Size	22.65	1	22.65	21.37	0.0024	
AB	72.68	1	72.68	68.56	< 0.0001	
AC	6.38	1	6.38	6.02	0.0439	
BC	0.4744	1	0.4744	0.4475	0.5250	
A^2	62.61	1	62.61	59.05	0.0001	
B^2	23.00	1	23.00	21.69	0.0023	
C^2	62.55	1	62.55	59.00	0.0001	
Residual	7.42	7	1.06			
Lack of Fit	7.05	5	1.41	7.66	0.1196	not significant
Pure Error	0.3685	2	0.1842			
Cor Total	3056.68	16				

R^2 = 0.9976, **Adjusted R^2** = 0.9945, **Predicted R^2** = 0.9802, **Adeq Precision** = 65.1991, **C.V.** = 2.31%

The baseline Coefficient of Determination (R^2) stands at an exceptional 0.9976, signifying that 99.76% of total variance is successfully explained by the model. High predictive fidelity is further verified by a Predicted R^2 of 0.9802 and an "Adequate Precision" signal-to-noise ratio of 65.1991, which vastly exceeds the mandatory threshold of 4.0.

3.2. Interpretation of Regression Coefficients and Multicollinearity

The VIF serves as a critical diagnostic tool designed to detect multi-collinearity—insidious instances where independent variables are highly correlated with one another. Multi-collinearity can artificially inflate the variance of the regression coefficients, completely destabilizing the predictive model. A VIF value equal to exactly 1.0 indicates absolute orthogonality (zero correlation) between factors. As clearly shown in Table 3, all linear and interaction terms possess a VIF of exactly 1.0000, and the quadratic terms exhibit a highly tolerable VIF of 1.29 (well below the universally accepted problematic threshold of 10). This definitive diagnostic proves that the central composite experimental design matrix was perfectly orthogonal. By explicitly maintaining this orthogonality, the reliability of the individual parameter effect estimations is significantly enhanced. It provides mathematical certainty that the calculated regression coefficient for any single factor reflects its pure, isolated impact on the response variable, unclouded by the confounding influence of the other factors. Consequently, every parameter's physical effect can be accurately interpreted and isolated without statistical cross-contamination.

Table 3. Coefficients in Terms of Coded Factors for Efficiency.

Factor	Coefficient Estimate	df	Standard Error	95% CI Low	95% CI High	VIF
Intercept	46.91	1	0.5680	45.57	48.26	
A-Torque	12.87	1	0.2574	12.26	13.48	1.0000
B-Bypass-angle	-2.45	1	0.2574	-3.05	-1.84	1.0000
C-Cone Size	-1.19	1	0.2574	-1.80	-0.5812	1.0000
AB	-3.01	1	0.3640	-3.87	-2.15	1.0000
AC	-0.8933	1	0.3640	-1.75	-0.0325	1.0000
BC	-0.2435	1	0.3640	-1.10	0.6173	1.0000
A^2	-1.80	1	0.2340	-2.35	-1.24	1.29
B^2	1.09	1	0.2340	0.5364	1.64	1.29
C^2	-1.80	1	0.2340	-2.35	-1.24	1.29

Based on verified orthogonal coefficients lacking multi-collinearity issues (Variance Inflation Factors below 1.29), the final predictive equation in terms of coded factors is articulated as eq. 5:

$$Y = 46.91 + 12.87 \text{ x } A - 2.45 \text{ x } B - 1.19 \text{ x } C - 3.01 \text{ x } AB - 0.8933 \text{ x } AC - 0.2435 \text{ x } BC - 1.80 \text{ x } A^2 + 1.09 \text{ x } B^2 - 1.80 \text{ x } C^2 \quad (5)$$

This mathematical model accurately translates dynamic physical behaviors within the turbine. The massive positive coefficient of factor A (Torque) with +12.87 indicates that the pure reaction turbine strictly requires significant mechanical load to efficiently extract kinetic energy. The negative linear effect of factor B (Bypass-angle) of -2.45 confirms that mechanically diverting fluid directly reduces the critical hydrostatic internal chamber pressure required for fluid acceleration through the restrictive nozzles. Crucially, factor C (Cone Size) exhibits an inverted-U parabolic curve defined by combined negative linear (-1.19) and quadratic (-1.80) effects. The statistical presence of this strong negative quadratic term is highly significant; it confirms that a true theoretical optimum exists within the evaluated design space, rather than a continuous linear trend that might simply terminate at an arbitrary experimental boundary. The experimental bounds—ranging from the $-\alpha$ extreme of 2.25 inches to the $+\alpha$ extreme of 3.25 inches—were explicitly structured to capture this physical transition point. If the internal cone is too small (approaching the lower bounds), turbulent stagnation zones continue to form; if it is too large (approaching the upper bounds), it severely constricts the internal flow cross-sectional area, acting as a massive internal throttle inducing severe frictional viscous dissipation. Therefore, the generated optimization model successfully envelopes the true hydrodynamic performance peak, validating that the bounds are sufficient to capture the absolute optimum rather than a mere localized maximum within a truncated range.

3.3. Diagnostic Plots and Model Validity

The validity of the chosen quadratic regression model was further evaluated through a series of standard diagnostic plots shown in Figure 3, ensuring that the fundamental assumptions of linear regression and ANOVA were satisfied. Figure 3(a) This standard probability plot demonstrates that the residuals are distributed approximately normally, as the plotted data points trace a relatively straight, diagonal line. This fulfills a primary assumption of the linear regression model. Figure 3(b), this plot exhibits a random scatter of residual points clustered around the zero line without a distinctive expanding or fanning pattern. This confirms homoscedasticity (constant variance of errors) and suggests the absence of unaccounted non-linear effects. Figure 3(c), by plotting the residuals against the chronological execution order of the experimental runs, the plot reveals random fluctuation. This validates the assumption of error independence, indicating that there were no discernible time-related drifts or carryover effects during the testing procedure. Figure 3(d), this plot illustrates a remarkably strong correlation between the efficiency values predicted by the mathematical model and the actual empirical data. The tight clustering of points along the 45-degree diagonal line signifies an excellent model fit and robust predictive accuracy.

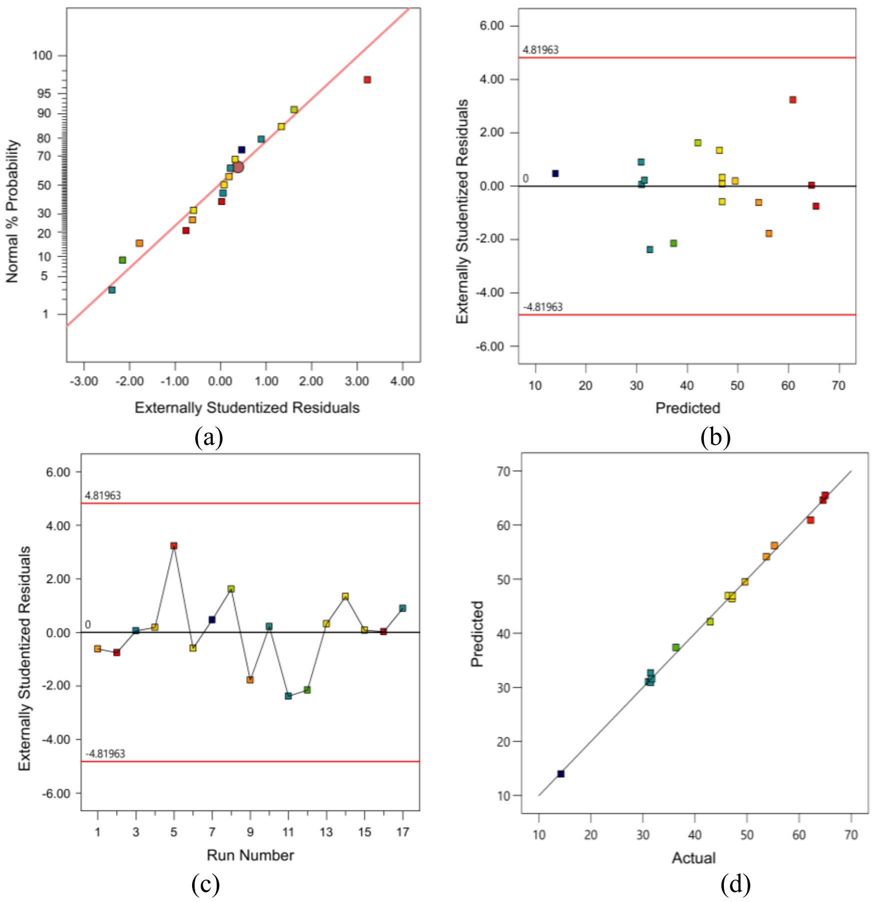

Fig. 3. The regression model's validity of CESRT, (a) Externally studentized residuals vs. Normal probability, (b) Predicted vs. Externally studentized residuals, (c) Number of runs vs. Externally studentized residuals and, (d) Actual vs. Predicted.

3.4. Analysis of Response Surface and Contour Plots

To visually interpret the complex, multi-variable interactions and their physical impact on the hydraulic efficiency of the 10-inch CESRT, 3D response surface and 2D contour plots were generated from the regression model.

Figure 4(a) illustrates the interactive response surface as a function of applied torque and bypass angle. The pronounced steepness of the surface explicitly along the torque axis visually confirms its status as the most dominant governing factor; efficiency climbs rapidly and linearly as torque increases from 20 N-m to 60 N-m. Furthermore, the contour lines clearly indicate that peak performance clusters heavily at the region of maximum torque combined with the minimum bypass angle (22.5°). This graphically reinforces the physical requirement that diverting flow away from the turbine via a high bypass severely penalizes the internal pressure needed for optimal momentum extraction.

Figure 4(b) depicts the interactive effects between the applied torque and the internal cone size. While the dominant, steepest gradient undeniably remains anchored along the torque axis, the curvature of the contour lines stretching across the cone size axis visually represents the significant quadratic effect (C^2) identified previously in the statistical model. At optimal high-torque conditions, the surface contour trends upward slightly as the cone size decreases toward the 2.5-inch boundary, indicating that this smaller geometry better balances flow vectoring against internal friction compared to the larger 3.0-inch extreme.

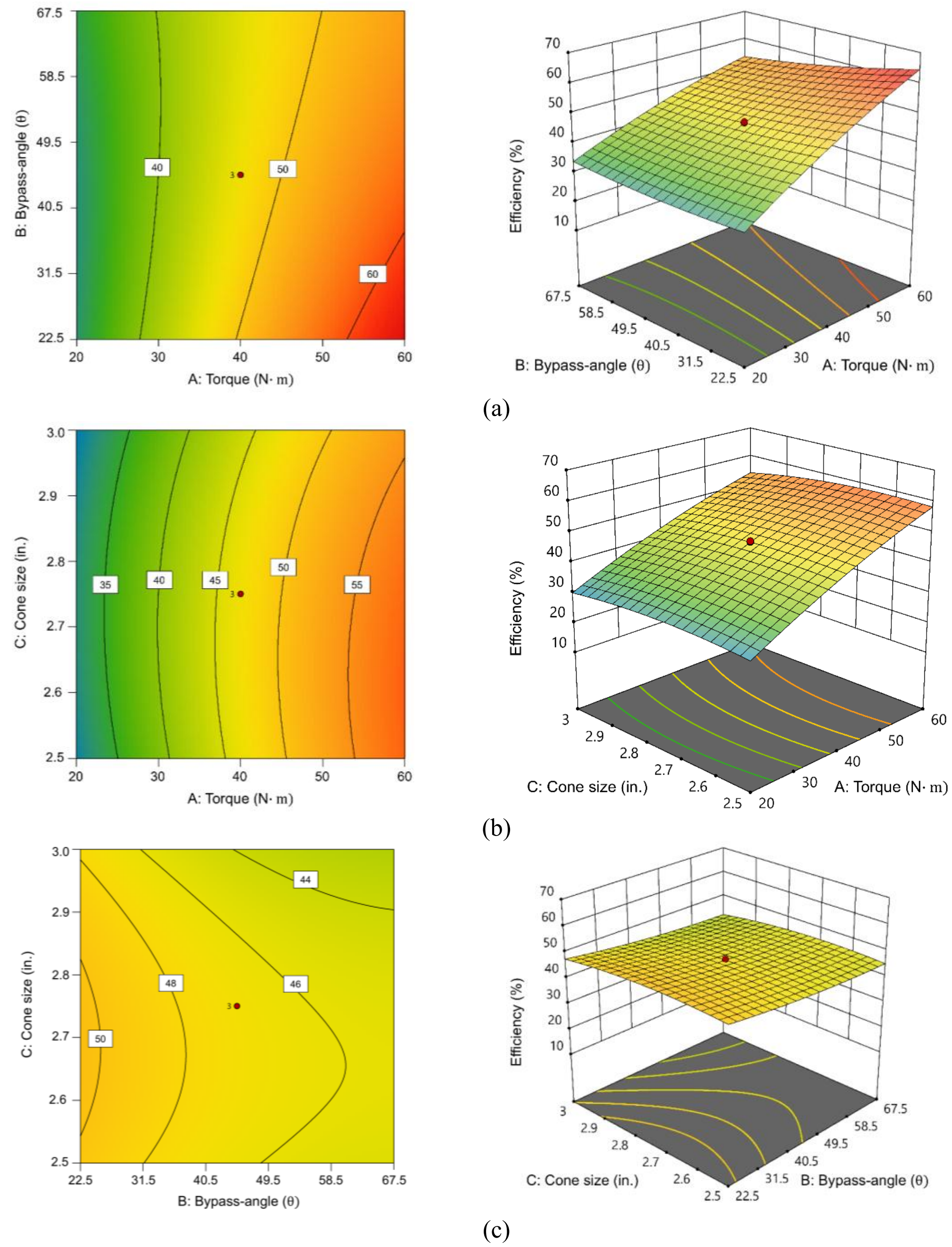

Fig. 4. The response surface and contour plots of efficiency as a function of torque (N-m) and bypass angle (θ) (a), torque (N-m) and cone size (in.) (b) and bypass angle and cone size (c).

Figure 4(c) presents the surface plot mapping bypass angle against cone size while rigidly holding the applied torque constant at its geometric center point (40 N-m). The relatively flat, undemanding topography of this specific surface plot visually corroborates the ANOVA findings, which mathematically deemed the interaction between bypass angle and cone size (BC) as statistically insignificant. The lack of severe surface twisting indicates that these two parameters act largely independently of one another. From a fluid dynamics perspective, this independence is rooted in the distinct physical roles each parameter plays within the system. The bypass angle primarily governs the absolute magnitude of the inlet mass flow and hydrostatic pressure by diverting fluid prior to chamber entry. In contrast, the internal cone size dictates the static geometric boundary conditions that define the internal streamline trajectories. Because the cone's primary hydrodynamic function is to vector flow radially outward and eliminate central stagnation zones, its geometric effectiveness is largely uncoupled from the incoming flow's velocity magnitude. The streamline geometry remains highly consistent, even as the volumetric flow rate fluctuates.

From a practical engineering and field-deployment perspective, this statistical and physical independence is highly advantageous. It implies that the internal cone geometry can be standardized and permanently fixed during fabrication without constraining the operator's ability to dynamically regulate the bypass angle in response to seasonal fluctuations in run-of-river flow rates. Essentially, field operators can modulate the inlet fluid dynamics via the bypass valve without fear of inducing unforeseen, detrimental hydrodynamic interactions with the static internal cone. However, the contour map still clearly directs the overall optimization trajectory toward the lowest possible bounds of both parameters to maximize the operational response.

3.5. Optimum Conditions for Efficiency and Desirability

The numerical optimization solution dictates that peak hydraulic efficiency for this specific architecture is realized when operating at the maximum bounded Torque (60 N-m), the minimum bounded Bypass-angle (22.5°), and the minimum bounded Cone Size (2.5 inches). Operating under this specific, highly constrained geometric and physical configuration yields a predicted peak isentropic efficiency of 64.5803%. The algorithm assigns this specific combination a perfect statistical desirability rating of 1.000, confirming it satisfies all target constraints and mathematically represents the absolute best performance achievable within the tested envelope as shown in Table 4.

Table 4. Optimal values of the designed factors for the 10.0-inch CESRT

Name	Goal	Lower Limit	Upper Limit	Optimum Value
A: Torque (N-m)	is in range	20	60	60
B: Bypass-angle (°)	is in range	22.5	67.5	22.5
C: Cone Size (in)	is in range	2.5	3	2.5
Efficiency (%)	Maximize	14.265	65.015	64.58%
Desirability		0	1	1

To visually represent this numerical optimization, a desirability ramp graph (Figure 5) was generated. This graph confirms the optimal operating coordinates, displaying the specific parameter ramps that culminate in the absolute maximum predicted efficiency of 64.5803% with an overall desirability score of 1.000 (identified as Solution 3 out of 100 generated possibilities).

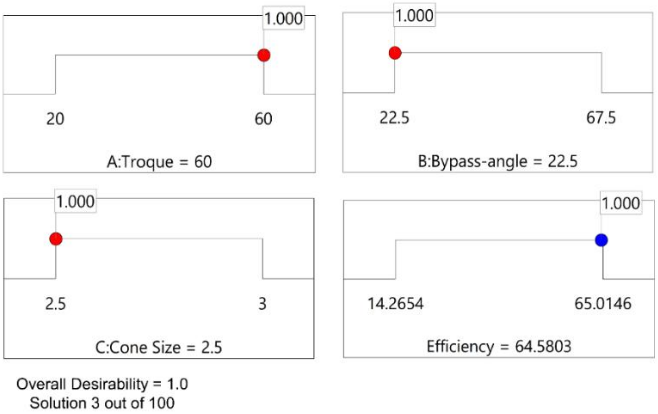

Fig. 5. Desirability for optimization of parameters for torque, bypass angle, cone size, and efficiency.

3.6. Comparative Hydrodynamic Scaling: The Aspect Ratio Penalty

In the highly controlled, foundational experiments conducted by Lastimado et al. (2025), an identical Split Reaction Turbine architecture—scaled to an 8-inch vertical height and optimized utilizing an identical CCD framework—achieved a remarkable peak efficiency of 77.0772% utilizing a 60 N-m torque, a 22.5° bypass angle, and a smaller 2.25-

inch cone. The present study, meticulously maintaining identical radial dimensions, identical fabrication materials, identical inlet boundary conditions, and identical statistical methodologies, but simply elongating the PVC housing vertically to 10 inches, achieves a maximum optimized efficiency of only 64.5803%.

This drastic, undeniable efficiency degradation of approximately 12.5 percentage points provides incontrovertible empirical evidence of the immense performance penalty associated with arbitrarily increasing the aspect ratio (height-to-diameter ratio) in simple reaction turbines (Teia, 2019). This phenomenon fundamentally challenges rudimentary assumptions about volumetric scaling and can be mathematically and physically deconstructed through three primary fluid dynamic loss mechanisms (Grönman & Uusitalo, 2021; Magayon et al., 2026):

1. Aggravation of Skin Friction and Viscous Dissipation: Aggravation of Skin Friction and Viscous Dissipation: Elongating the turbine housing from 8 inches to 10 inches inherently and unavoidably increases the total internal wetted surface area of the cylindrical PVC housing by a massive 25%. In enclosed, pressurized fluid passages, fluid velocity directly at the boundary wall is zero (the foundational no-slip condition). As pressurized fluid moves axially from the bottom inlet orifice toward the top of the chamber, viscous shear forces propagate inward from the rotating PVC walls, causing a drag-inducing boundary layer to grow. This degradation can be quantitatively contextualized using the classical Darcy-Weisbach theoretical model for internal pipe flow, where frictional head loss (h_f) is directly proportional to the passage length (L) via the relation $h_f = f(L/D)(V^2/2g)$. By elongating the turbine housing from 8 inches to 10 inches while maintaining a constant internal diameter (D), the length variable (L) is mathematically increased by 25%. Consequently, the theoretical frictional head loss imposed on the vertical fluid column scales proportionately. A much larger fraction of the fluid's initial kinetic energy and potential pressure head is irreversibly dissipated into heat via viscous friction along the walls, rather than being preserved to generate reactive thrust at the nozzle exits (Babaiasl et al., 2020; Song et al., 2024).

2. Decoupling of Flow Vectoring and Internal Stagnation: The foundational engineering premise of the Cone-Enhanced Split Reaction Turbine is that the static conical insert physically intercepts the incoming vertical water column, aggressively and smoothly turning 90 degrees outward to feed the vertical exit nozzles with minimal flow separation or turbulence. In the compact 8-inch turbine, the physical proximity of the top and bottom cover plates intrinsically compresses the internal flow, and the optimized 2.25-inch cone effectively occupies the necessary internal volume to force the fluid outward smoothly.

However, in the elongated 10-inch housing, the internal cavity volume is significantly expanded. Even with the newly optimized, larger 2.5-inch cone, the massive aspect ratio of the cavity fundamentally alters the internal flow vectors. The fluid stream entering from the base possesses sufficient unobstructed volume to physically separate from the guiding surfaces of the cone. This separation inevitably leads to the formation of massive, highly energetic recirculating vortices (dead zones) in the vast upper extremities of the 10-inch pipe. These vortices trap pressurized fluid in endless rotational loops within the upper housing, acting as massive parasitic hydraulic loads that rob the entire system of potential mechanical energy (Harun et al., 2020; Hasan et al., 2020).

3. Kinetic Energy Dilution and Exit Acceleration Penalties: For a constant volumetric flow rate (Q) dictated by the run-of-river source or the test pump, a geometric increase in the internal volume of the turbine body strictly correlates to a massive decrease in the mean internal fluid velocity (V = Q/A). While the exit nozzle cross-sectional area remains completely constant across both the 8-inch and 10-inch designs, the larger internal volume of the 10-inch cylinder drastically decelerates the fluid as it enters the main chamber. The water must then undergo a much more extreme, violent, and rapid acceleration to exit the restrictive split nozzles. This rapid, chaotic acceleration from a slower, more turbulent internal state introduces massive, localized pressure drops right at the nozzle entrance lip, heavily penalizing the smooth, isentropic expansion process strictly required for maximum reactive thrust generation.

Consequently, the optimization algorithm for the 10-inch model mathematically "chose" a 2.5-inch cone as the optimum (significantly larger than the 2.25-inch optimum of the 8-inch model) in a desperate hydrodynamic attempt to plug the expanded internal volume and mechanically force the sluggish, decelerated fluid out the nozzles. However, this larger cone inherently introduces its own massive blockage penalties, resulting in the severely depressed 64.5803% absolute efficiency ceiling.

To explicitly benchmark this 12.5% efficiency degradation against other prevailing low-head hydrokinetic technologies, it is highly instructive to compare these results against axial-flow systems such as the Archimedean Screw Turbine (AST). In AST architectures, elongating the central axis (increasing the length-to-diameter ratio) generally correlates with a stabilization or an *increase* in isentropic efficiency, as a longer helical flight surface captures a larger total pressure gradient and minimizes volumetric fluid leakage per unit of length (Sobel et al., 2025). The empirical data demonstrating that the CESRT exhibits the exact opposite behavioural trend—a severe efficiency degradation upon vertical elongation—categorically proves that unguided radial reaction turbines operate on fundamentally inverted geometric scaling principles compared to axial low-head machines. In reaction turbines, the primary energy conversion mechanism is centrifugal and tangential, strictly governed by the radial plane; thus, extending the vertical axial length merely introduces a massive parasitic friction penalty and flow separation zone without any corresponding energy extraction benefit (Bagheri-Sadeghi et al., 2021)

Crucially, the empirically observed aspect ratio penalty is not an isolated aerodynamic anomaly specific only to the CESRT architecture; rather, it establishes a universal hydrodynamic heuristic applicable to the broader class of simple, outward-radial flow reaction turbomachinery (encompassing Barker's mills, Z-pipe turbines, and unguided SRT variants). In all such pure reaction systems, the extraction of angular momentum is exclusively dependent on the radial moment arm governing the tangential exit nozzles, governed by the conservation of angular momentum where torque is a product of mass flow rate, radial distance, and tangential velocity vector. Geometrically elongating the vertical axis universally violates the machine's optimal power density by continuously inflating internal viscous losses and instigating flow decoupling, all without contributing any additional mechanical leverage for torque generation. This stands in stark contrast to specific low-head axial-flow architectures (such as Archimedean screws or micro-Kaplan variants), where axial elongation can inherently correlate with increased head utilization or prolonged fluid interaction. Consequently, these findings mathematically define a rigid boundary condition for the field of decentralized fluid power: for simple, unguided reaction topologies, volumetric power scaling must universally prioritize radial expansion over vertical elongation. The absolute necessity for radial expansion over vertical elongation is not merely an empirical observation of the CESRT, but a direct validation of the fundamental Euler turbomachine equation. In any pure reaction turbine, the mechanical torque (T) extracted from the fluid is fundamentally proportional to the mass flow rate ($\dot{m}$) and the change in angular momentum, heavily dictated by the radial distance (r) of the fluid discharge nozzle from the central axis of rotation: $T = \dot{m}\Delta(rc_\theta)$. By expanding the turbine radially, the design directly increases this critical moment arm (r), exponentially increasing potential torque extraction for a given mass flow rate without inherently requiring higher fluid velocities (Talluri et al., 2021). Conversely, vertical elongation fundamentally ignores the r variable in the Euler equation. It forces the system to accommodate a larger internal volumetric capacity without providing any additional mechanical leverage at the periphery. Consequently, global design heuristics for low-cost, unguided reaction turbines must dictate that any required increase in internal capacity be achieved through expanding the radial envelope, thereby satisfying both the conservation of angular momentum and the minimization of parasitic boundary layer growth.

4. Conclusion

This comprehensive research provides a rigorous, data-driven parameter optimization and hydrodynamic scaling analysis of a novel 10-inch Cone-Enhanced Split Reaction Turbine (CESRT), specifically targeted for deployment in sustainable, ultra-low-head pico-hydropower systems. Through the execution of a highly robust Central Composite Design (CCD) experimental framework nested within a Response Surface Methodology (RSM) analysis, the study successfully mapped the complex, highly non-linear hydrodynamic interactions between applied mechanical torque, fluid bypass angle, and internal geometric cone sizing. This specific methodology was critical in addressing the inherent complexities of the fluid system; unlike traditional one-factor-at-a-time (OFAT) or linear models that assume purely proportional relationships, the CCD matrix—by incorporating strategically placed axial and center points—provided the precise mathematical scaffolding required to detect and quantify severe parabolic curvature.

Consequently, the analysis definitively determined that the multi-variable design space is accurately and reliably modeled by a second-order quadratic polynomial, validated by exceptional statistical fit metrics including an overwhelming model F-value of 319.59 and a highly robust predictive R^2 of 0.9802. This advanced modeling framework enabled the explicit identification of non-linear phenomena, such as the inverted-U efficiency degradation associated with boundary cone sizing, ensuring that the true theoretical peak was successfully captured. Mathematical numerical optimization revealed that absolute maximum system efficiency is strictly achieved under high mechanical loading (60 N-m torque), maximal fluid delivery (a 22.5° bypass angle constraint), and a tightly controlled internal flow geometry utilizing a 2.5-inch cone, yielding a peak hydraulic efficiency of 64.5803%.

This study establishes a critical, mathematically proven engineering heuristic for the future development of sustainable pico-hydro reaction turbines: volumetric scaling efforts must absolutely eschew vertical elongation in favor of radial expansion. Doing so maximizes reactive thrust moment arms while preserving vital boundary layer attachment and isentropic flow integrity. Crucially, this fundamental geometric scaling rule transcends the specific CESRT architecture, providing a universal design constraint applicable to a diverse spectrum of simple, outward-flow reaction machines, including Z-pipe turbines, Barker's mills, and unguided split-pipe configurations. By applying this radial-centric heuristic, these technologies can be reliably scaled to accommodate a wide array of operational environments—from variable run-of-river streams to agricultural irrigation outfalls—without suffering catastrophic viscous degradation. Ultimately, these definitive findings equip the global engineering community and field practitioners with the rigorous theoretical framework necessary to confidently scale and deploy ultra-low-cost, highly efficient, decentralized energy solutions for off-grid communities worldwide.

References

A, S. D. (2023). Response Surface Methodology-A Statistical Tool for the Optimization of Responses. *Global Journal of Addiction & Rehabilitation Medicine*, *7*(1). https://doi.org/10.19080/gjarm.2023.07.555705

Babaiasl, M., Boccelli, S., Chen, Y., Yang, F., Ding, J., & Swensen, J. (2020). Predictive mechanics-based model for depth of cut (DOC) of waterjet in soft tissue for waterjet-assisted medical applications. *Medical & Biological Engineering & Computing*, *58*(8), 1845–1872. https://doi.org/10.1007/s11517-020-02182-0

Bagheri-Sadeghi, N., Helenbrook, B. T., & Visser, K. D. (2021). Maximal power per device area of a ducted turbine. *Wind Energy Science*, *6*(4), 1031–1041. https://doi.org/10.5194/wes-6-1031-2021

Barsi, D., Ubaldi, M., Zunino, P., & Fink, R. (2019). A new compact hydraulic propeller turbine for low heads. *E3S Web of Conferences*, *116*, 5–5. https://doi.org/10.1051/e3sconf/201911600005

Chica, E., & Rubio-Clemente, A. (2017). Design of Zero Head Turbines for Power Generation. In *InTech eBooks*. https://doi.org/10.5772/66907

Grönman, A., & Uusitalo, A. (2021). Analysis of radial-outflow turbine design for supercritical CO2 and comparison to radial-inflow turbines. *Energy Conversion and Management*, *252*, 115089–115089. https://doi.org/10.1016/j.enconman.2021.115089

Harun, Z., Oyegbile, B., Oyegbile, B., Akdogan, G., Oyegbile, B., Oyegbile, B., Abrahamyan, M. G., Yoshikawa, S., Song, L., Nikolaev, E. I., Nikolaeva, M., & Mori, M. (2020). Vortex Dynamics Theories and Applications. In *IntechOpen eBooks*. IntechOpen. https://doi.org/10.5772/intechopen.87912

Hasan, M. K., Manasseh, R., & Leontini, J. S. (2020). Energy loss and developing length during reciprocating flow in a pipe with a free-end. *Physics of Fluids, 32*. https://doi.org/10.1063/5.0011701

Hunt, A., Stringer, C., & Polagye, B. (2020). Effect of aspect ratio on cross-flow turbine performance. *arXiv (Cornell University)*, *12*(5). https://doi.org/10.1063/5.0016753

Hunt, A., Strom, B., Talpey, G., Ross, H., Scherl, I., Brunton, S. L., Wosnik, M., & Polagye, B. (2024). An experimental evaluation of the interplay between geometry and scale on cross-flow turbine performance. *Renewable and Sustainable Energy Reviews*, *206*, 114848–114848. https://doi.org/10.1016/j.rser.2024.114848

Ibekwe, K. I., Etukudoh, E. A., Nwokediegwu, Z. Q. S., Umoh, A. A., Adefemi, A., & Ilojianya, V. I. (2024). ENERGY SECURITY IN THE GLOBAL CONTEXT: A COMPREHENSIVE REVIEW OF GEOPOLITICAL DYNAMICS AND POLICIES [Review of *ENERGY SECURITY IN THE GLOBAL CONTEXT: A COMPREHENSIVE REVIEW OF GEOPOLITICAL DYNAMICS AND POLICIES*]. *Engineering Science & Technology Journal*, *5*(1), 152–168. Fair East Publishers. https://doi.org/10.51594/estj.v5i1.741

Journals, I., Nimje, A. A., & Dhanjode, G. (2015). Pico-Hydro-Plant for Small Scale Power Generation in Remote Villages. *Figshare*. https://doi.org/10.6084/m9.figshare.1344715

Kayarogannam, P., Njoku, C. N., Otisi, S. K., Lamidi, S., Olaleye, N., Bankole, Y., Obalola, A., Aribike, E., Adigun, I., Nguyen, N., Borkowski, J. J., Vuong, M. P., Ahmad, A., Alam, S., Sharma, M., & Sağbaş, A. (2022). Response Surface Methodology - Research Advances and Applications. In *IntechOpen eBooks*. IntechOpen. https://doi.org/10.5772/intechopen.102317

Lange, K., Wehrli, B., Åberg, U., Bätz, N., Brodersen, J., Fischer, M., Hermoso, V., Liermann, C. R., Schmid, M., Wilmsmeier, L., & Weber, C. (2019). Small hydropower goes unchecked [Review of *Small hydropower goes unchecked*]. *Frontiers in Ecology and the Environment*, *17*(5), 256–258. Wiley. https://doi.org/10.1002/fee.2049

Lastimado, A. E., Jr, Siasico, W. O., Posada, J. D., et al. (2025). Performance optimization sof a cone enhanced split reaction turbine by response surface methodology. *International Journal of Engineering Trends and Technology, 73*(8), 75–90. https://doi.org/10.14445/22315381/IJETT-V73I8P106

Lastimado, A. E., Pahunang, R. R., Rabongue, A., et al. (2025). Acid-salt-modified natural zeolite as a highly efficient adsorbent for pharmaceuticals from contaminated water. *Journal of Water Process Engineering, 79*, 109065.

Magayon, C. M., Salinas, J. P. P., Maquilan, M. C. L., & Jr, A. E. L. (2026). Optimizing a lab-scale Savonius wind turbine via central composite design. *International Journal of Mechanical Engineering Education*. https://doi.org/10.1177/03064190261448795

Mansour, G., Papageorgiou, V., & Tzetzis, D. (2024). Carbon Fiber Polymer Reinforced 3D Printed Composites for Centrifugal Pump Impeller Manufacturing. *Technologies*, *12*(4), 48–48. https://doi.org/10.3390/technologies12040048

Mohammed, M., Alqahtani, N. K., & Ali, S. (2024). Development, RSM-based modeling, and process optimization of an ultrasonic coating system for extending the storage life of fresh fruits. *Frontiers in Sustainable Food Systems, 8*. https://doi.org/10.3389/fsufs.2024.1403164

Njoku, C. N., & Otisi, S. K. (2023). Application of Central Composite Design with Design Expert v13 in Process Optimization. In *IntechOpen eBooks*. IntechOpen. https://doi.org/10.5772/intechopen.109704

Palanikumar, K. (2021). Response Surface Methodology in Engineering Science. *IntechOpen*. https://doi.org/10.5772/intechopen.90965

Sebastián, A., Abbas, R., & Valdés, M. (2021). Analytical prediction of Reynolds-number effects on miniaturized centrifugal compressors under off-design conditions. *Energy*, *227*, 120477–120477. https://doi.org/10.1016/j.energy.2021.120477

Sobel, J. B., Buhia, J., & Tino, C. (2025). Performance Optimization of an Archimedean Screw Turbine a Hydropower Generator for Sustainable Energy Generation. *International Journal of Mechanical Engineering, 12*. https://doi.org/10.14445/23488360/ijme-v12i10p107

Song, J., Wang, S., Qiu, Z., Peng, D., Liu, Y., & Wen, X. (2024). Flow mechanism study and geometrical parameters analysis of fluidic oscillators based on pressure-sensitive paint measurements and modal analysis. *Experiments in Fsluids*, *65*(3). https://doi.org/10.1007/s00348-024-03773-5

Subekti, R. A., Prawara, B., Susatyo, A., Fudholi, A., Wijaya, S. K., & Sudarmaji, A. (2022). Design and performance of very low head water turbines using a surface vorticity model algorithm. *International Journal of Power Electronics and Drive Systems/International Journal of Electrical and Computer Engineering*, *13*(2), 1140–1140. https://doi.org/10.11591/ijpeds.v13.i2.pp1140-1149

Talluri, L., Niknam, P. H., Copeta, A., Amato, M. P., Iora, P., Uberti, S., Invernizzi, C. M., Marcoberardino, G. D., Pacini, L., Manfrida, G., & Fiaschi, D. (2021). A revised Tesla Turbine concept for 2-phase applications. *E3S Web of Conferences*, *238*, 10006–10006. https://doi.org/10.1051/e3sconf/202123810006

Teia, L. (2019). New Insight Into Aspect Ratio's Effect on Secondary Losses of Turbine Blades. *Journal of Turbomachinery, 141*. https://doi.org/10.1115/1.4044079

Williamson, S., Lubitz, W. D., Williams, A., Booker, J. D., & Butchers, J. (2019). Challenges Facing the Implementation of Pico-Hydropower Technologies. *Journal of Sustainability Research*, *2*(1). https://doi.org/10.20900/jsr20200003

Yeswanth, Mr. A. (2025). Face Centered Central Composite Design to Optimize The Material Extrusion Process. *International Journal of Science Engineering and Technology*, *13*(2), 1–9. https://doi.org/10.61463/ijset.vol.13.issue2.250

Zhussupbekov, M., Wu, J. X., Burgreen, G. W., et al. (2025). Multi-Objective CFD Optimization of an Intermediate Diffuser Stage for PediaFlow Pediatric Ventricular Assist Device. *PubMed*. https://doi.org/10.1111/aor.70004